Unsteady Numerical Simulation of the Turbulent Flow around an Exhaust Valve

M. Žaloudek, H. Deconinck, and J. Fořt

Abstract The article presents numerical results of the flow which is exhausted from the combustion chamber of a four-stroke engine. The unsteady simulations shown correspond to one working cycle of an exhaust valve.

The flow has been described by the set of Reynolds–averaged Navier–Stokes equations. The working medium has been assumed an ideal gas. The numerical solution has been acquired with an in-house numerical code, *COOLFluiD*, based on a finite volume method (FVM). The numerical code is being developed by the team of engineers with wide range of specialization. Our major contribution has been connected to the implementation of the advanced turbulence models for both steady and unsteady simulations on moving grids.

The current work focuses on the turbulence modelling and on the simulation of the real valve movement. The flow structure and the mass flow rate are observed.

Due to a lack of experimental data, the computations are performed in a stepwise manner, validating each implementation step on the testcases known, before being applied to the valve geometry. The results presented therefore correspond to a planar model. The article focuses on the implementation of turbulence models and their application to complex geometry problems, rather than exploring new numerical methods.

Keywords numerical simulation, exhaust systems, turbulence
MSC2010: 76N15, 76F55, 76H05

Milan Žaloudek and Jaroslav Fořt
Dept. of Technical Mathematics, Czech Technical University, Karlovo nám. 13, CZ-12135 Praha 2, e-mail: Milan.Zaloudek@fs.cvut.cz, Jaroslav.Fort@fs.cvut.cz

Herman Deconinck
von Kármán Institute for Fluid Dynamics, Chaussée de Waterloo 72, B-1640 Rhode-Saint-Genèse, e-mail: deconinck@vki.ac.be

J. Fořt et al. (eds.), *Finite Volumes for Complex Applications VI – Problems & Perspectives*, Springer Proceedings in Mathematics 4,
DOI 10.1007/978-3-642-20671-9_83, © Springer-Verlag Berlin Heidelberg 2011

1 RANS Equations

The flow is governed by conservation laws of mass, momentum and energy and two transport equations of the turbulence model.

$$\frac{\partial \mathbf{W}}{\partial t} + \frac{\partial \mathbf{F}_i^I}{\partial x_i} = \frac{\partial \mathbf{F}_i^V}{\partial x_i} + \mathbf{Q}\,, \tag{1}$$

with t representing time, $\mathbf{x}$ the Cartesian coordinates, $\mathbf{W}$ the vector of conservative unknowns, $\mathbf{F}^I/\mathbf{F}^V$ the convective/viscous fluxes and $\mathbf{Q}$ the source term.

$$\mathbf{W} = |\rho\,,\ \rho w_1\,,\ \rho w_2\,,\ e\,,\ \rho k\,,\ \rho\omega|^T \tag{2}$$

$$\mathbf{F}_i^I = w_i\,|\rho, \rho w_1 + \tilde{p}\delta_{i1}, \rho w_2 + \tilde{p}\delta_{i2}, e + \tilde{p}, \rho k, \rho\omega|^T$$

$$\mathbf{F}_i^V = \left|0, \tau_{i1}, \tau_{i2}, \tau_{ij} w_j - q_i - q_i^t, (\mu + \sigma_k \mu_t)\,\frac{\partial k}{\partial x_i}, (\mu + \sigma_\omega \mu_t)\,\frac{\partial \omega}{\partial x_i}\right|^T$$

$$\mathbf{Q} = \left|0, 0, 0, 0, P - \beta^* \rho k \omega, \frac{\gamma}{\nu_t} P - \beta \rho \omega^2 + (1 - F_1)\,\rho \frac{2\sigma_2}{\omega}\frac{\partial k}{\partial x_j}\frac{\partial \omega}{\partial x_j}\right|^T$$

The unknows ρ, $\mathbf{w} = (w_1; w_2)$, e, p, T, k, ω denote in turns the density, the velocity components, the total energy, the pressure, the temperature, the turbulent kinetic energy and the specific dissipation rate. The stress tensor τ_{ij} is expressed as

$$\tau_{ij} = (\mu + \mu_t)\,S_{ij}\ ,\ S_{ij} = \frac{1}{2}\left(\frac{\partial w_i}{\partial x_j} + \frac{\partial w_j}{\partial x_i}\right) - \frac{2}{3}\cdot\delta_{ij}\cdot\frac{\partial w_k}{\partial x_k}\,, \tag{3}$$

with δ_{ij} the Kronecker delta and μ, μ_t the molecular and turbulent dynamic viscosity

$$\mu = \frac{C_1 T^{3/2}}{T + S}\ ,\ \mu_t = \gamma^* \rho \frac{k}{\omega}\,. \tag{4}$$

The heat flux and the production term read

$$q_i = -\frac{\lambda}{\mathrm{Pr}}\frac{\partial T}{\partial x_i}\,,\ q_i^t = q_i \frac{\mathrm{Pr}}{\mu}\frac{\mu_t}{\mathrm{Pr}_t}\,,\ P = \mu_t S_{ij} S_{ij}\,. \tag{5}$$

Unknowns $\sigma_k, \sigma_\omega, \beta, \beta^*, \gamma, \gamma^*, \sigma_2, C_1, S, \lambda$ represent various constants to be found in the literature [7] and Pr stands for the Prandtl number. The function F_1 provides a blending between the $k-\epsilon$ model in freestream regions and the $k-\omega$ model near the wall surfaces. The system is completed with the state equation. The next turbulence models presented, have used a similar formulation as (1) and their specifics have been published in [10] (EARSM model) and [11] (Wilcox $k-\omega$, rev. 2008).

ALE Formulation. For unsteady simulations with a moving valve the arbitrary Lagrangian–Eulerian formulation of the RANS equations has been used, see [9]. The relative velocity $\mathbf{w}_R$ is defined as

$$\mathbf{w}_R = \mathbf{w} - \mathbf{w}_V \,, \tag{6}$$

with $\mathbf{w}$ the flow velocity and $\mathbf{w}_V$ the velocity of the valve (given by the movement imposed, see fig. 6). The convective flux $\mathbf{F}^I$ is then updated to a form

$$\mathbf{F}_i^{I,ALE} = w_{iR} \, |\rho, \rho w_1 + \tilde{p}\delta_{i1}, \rho w_2 + \tilde{p}\delta_{i2}, e + 2\tilde{p}, \rho k, \rho\omega|^T \tag{7}$$

2 Mathematical Formulation

The system (1) is solved upon the computational domain, see the Fig. 1. Although the real configuration is fully 3D, the computational domain has been considered symmetric with respect to the valve axis. Hence, only a half of the domain has been solved. A mathematic solution fulfils the equation (1) upon the domain interior, the *initial condition* at $t = 0$ and the following *boundary conditions* on the domain borders:

inlet total pressure, total temperature, incidence angle, turbulent variables according to the paper [8]:

$$\omega^{in} = \frac{|\mathbf{w}^{in}|}{L_{ref}}, \quad k^{in} = \omega^{in} \cdot \frac{\mu_\infty}{100} \,. \tag{8}$$

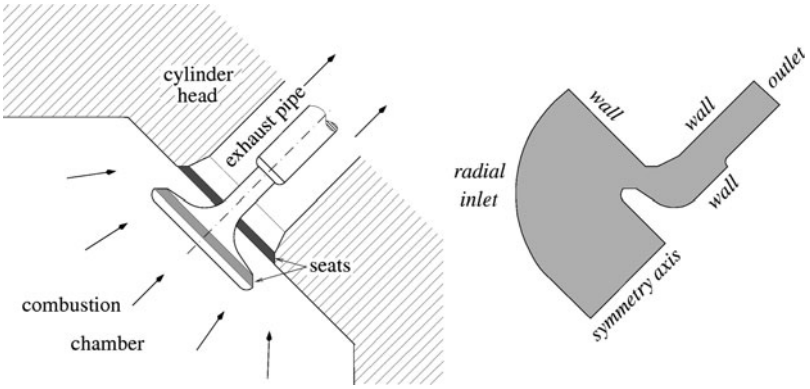

Fig. 1 Detail of the exhaust valve (left), scheme of the computational domain (right)

outlet pressure, velocity, temperature and turbulent variables

$$p = p^{out} \ , \ \frac{\partial w_i}{\partial n} = \frac{\partial T}{\partial n} = \frac{\partial k}{\partial n} = \frac{\partial \omega}{\partial n} = 0 \tag{9}$$

wall the adiabatic no-slip condition. The turbulent variables use the expressions suggested at [8]

$$\mathbf{w} \equiv 0, \ \frac{\partial T}{\partial n} = 0, \ k^w = 0, \ \omega^w = \frac{60\nu}{\beta_1 y_0^2} \tag{10}$$

3 Discretization and Numerical Method

The computational domain has been discretized by a structured triangular grid, see the Fig. 2. The steady flow computations were achieved with the time marching method based on a finite volume method, discretizing the equations (1) as

$$\frac{W_i^{n+1} - W_i^n}{\Delta t} = \frac{1}{\mu_i} \sum_{k=1}^{\#faces} \left(-\tilde{F}_k^I \cdot \mathbf{n}_k + \tilde{F}_k^V \cdot \mathbf{n}_k \right) , \tag{11}$$

with μ_i the area of the i-th volume, $\tilde{F}_k^I / \tilde{F}_k^V$ the numerical approximation of the advection/viscous fluxes and $\mathbf{n}_k$ the unit outward normal vector to the k-th face of the volume i. The fully implicit time integration has been used

$$W_i^{n+1} = W_i^n + \frac{\Delta t}{\mu_i} \sum_{k=1}^{\#faces} \left(-\tilde{F}^I \left(W^n, \, W^{n+1} \right)_k \cdot \mathbf{n}_k + \tilde{F}^V \left(W^n, \, W^{n+1} \right)_k \cdot \mathbf{n}_k \right) , \tag{12}$$

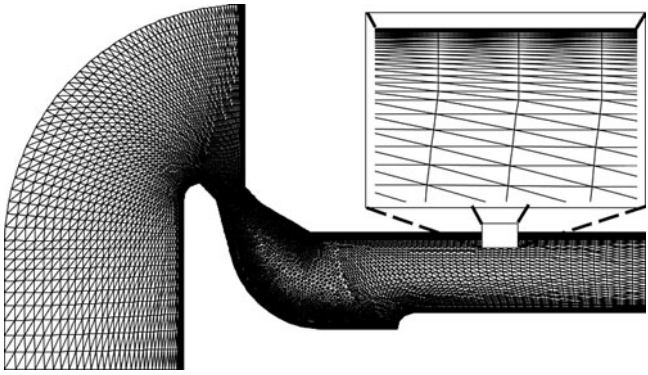

Fig. 2 Overview of the computational grid with the detail of its structure

as it is described in [5]. The linear system has been solved numerically by the GMRES iterative solver, provided by the PETSc library. As the flowfield contains both regions with the gas of negligible velocity (inside the chamber, Mach number ≈ 0.05) and regions with the gas of supersonic velocity (between the seats, $M \approx 2.0$) the numerical scheme $AUSM^{+up}$ able to capture all the velocity scales has been used. The algorithm is based on a solution of the Riemann problem (flux over a discontinuous step between two states) and thanks to the pressure and Mach number correction terms it improves the convergence also for the low velocity regions. The scheme has been published in [6]. The viscous fluxes have been computed as a central approximation, using a diamond dual cell approach.

The spatial accuracy has been improved by a piecewise linear reconstruction that has been built by the least squares interpolation method, complemented with the Barth limiter [2].

Unsteady Flow. The computational domain (and grid) changes with the advancing time. The solution is therefore based on the ALE formulation for moving grids. In order to avoid the situation of two disjunct subdomains with no flow between them for the closed valve a minimal valve opening (treshold) has always been used. Later, due to the significant grid deformation the domain has been remeshed and the current solutions interpolated in a conservative way. The series of three meshes (initial valve lift: 0.5 mm, 2.5 mm, 7.0 mm) have been used to resolve one working cycle of the exhaust valve.

The steady computations algorithm is modified to ensure the accuracy and consistency also for the unsteady flow. The time accurate solution has been obtained with the dual time stepping technique, consisting of an *outer time stepping loop* for a real time-accurate time step Δt and an *inner time stepping loop* with a fictitious time step τ to solve the system at each real time step. For the initiation phase the single step Crank–Nicholson method has been used, followed by the backward differentiation formula BDF2

$$\frac{W^{n+1,\alpha+1} - W^{n+1,\alpha}}{\tau} + \frac{3W^{n+1,\alpha+1} - 4W^{n} + W^{n-1}}{2\Delta t} = \tag{13}$$

$$\frac{1}{\mu_i} \sum_{k=1}^{\#faces} \left[\tilde{F}^V \left(W^n, W^{n+1,\alpha}, , W^{n+1,\alpha+1} \right)_k \cdot \mathbf{n}_k - \tilde{F}^I \left(W^n, W^{n+1,\alpha}, , W^{n+1,\alpha+1} \right)_k \cdot \mathbf{n}_k \right]$$

4 Steady Flow Numerical Results

The Fig. 3 reveals the steady solutions with different turbulence models. The computations have been stated by the parameters: valve opening 4 mm, temperature 500 K, pressure ratio $\frac{p_{inlet}}{p_{outlet}} = 2.5$, with the outlet pressure 100 kPa, corresponding to the exhaust to the atmosphere. The flow topology is similar for all models, consisting of a main beam (in approximately same position), surrounded by separation zones on both sides. The differences are visible on the pressure distribution along a streamline that passes the middle of a channel throat, see the Fig. 4. The BSL and

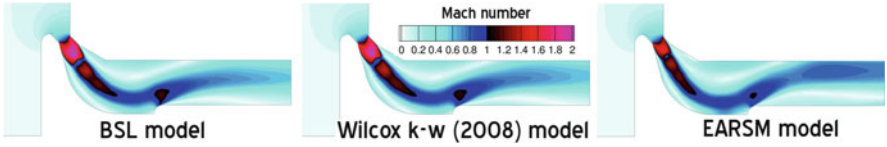

Fig. 3 Contours of Mach number for various turbulence models

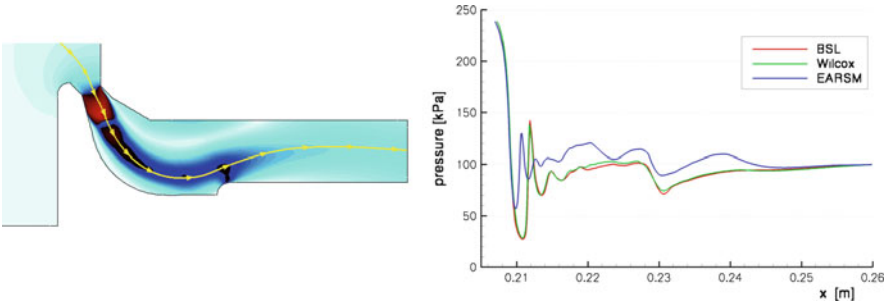

Fig. 4 The streamline for extracting the flow characteristics (left), comparison of the pressure through the exhaust pipe (right)

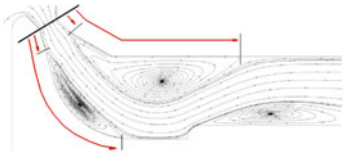

	lower wall [mm]			upper wall [mm]		
	start	end	length	start	end	length
BSL	2.8231	21.237	18.414	2.8284	35.730	32.901
Wilcox	2.1243	22.024	19.899	2.8284	35.774	32.945
EARSM	0.3643	18.091	17.727	0.0000	34.873	34.873

Fig. 5 Position of separation zones meassured from the channel throat

Wilcox models have a similar nature, which justifies similar results achieved by these models. By the contrary, the EARSM model allows anisotropic turbulence, see [10], leading to the milder peaks predicted and higher outlet velocity. However, the qualitative agreement is observed across all the models. Similar behaviour can be seen also on the comparison of the separation zone positions in the Table 5.

The next expansion is allowed due to the separations which form an artificial nozzle-like channel inside the exhaust pipe. These separations are described in the Fig. 5.

5 Unsteady Flow Numerical Results

The movement of the exhaust valve is shown in the Fig. 6a (valve lift vs. time). The next graph, Fig. 6b, shows the time evolution of the inlet pressure for a spark-ignition (SI), a compression-ignition (CI) engine and the outlet pressure. Values are taken from [4] and represent the boundary conditions for the unsteady simulations.

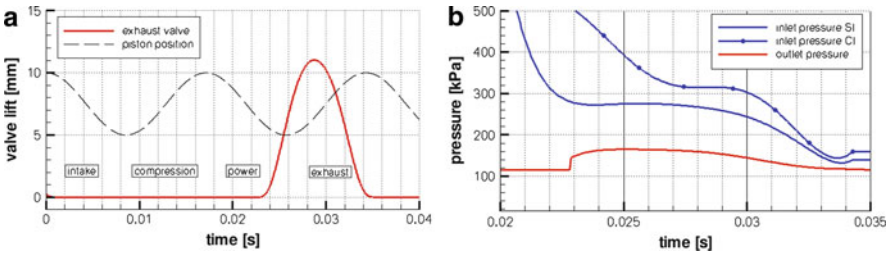

Fig. 6 The movement of the exhaust valve (left), the operating conditions at the inlet and outlet (right)

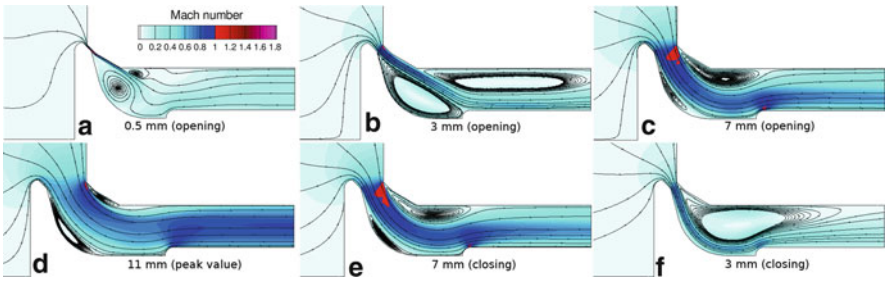

Fig. 7 SI engine. Contours of Mach number, velocity streamlines

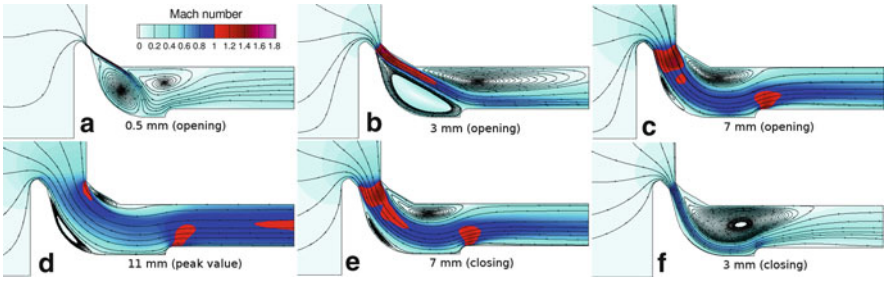

Fig. 8 CI engine. Contours of Mach number, velocity streamlines

The computations start at $t = 0.022$ (see Fig. 6) and the exhaust valve cycle lasts approximately 0.015 seconds. This interval has been resolved with the timestep $\Delta t = 10^{-6}\,s$ and with a valve lift treshold 0.5 mm. The results of the unsteady computations correspond to the valve lifts: $0.5 \rightarrow 3 \rightarrow 7 \rightarrow 11 \rightarrow 7 \rightarrow 3$ mm for both SI and CI inlet pressure evolutions.

The lift 7 mm has also been supplied by a pair of steady computations at boundary condition of the CI engine for the given lift, see the Fig. 9. The last Fig. 10 shows the mass flow rate over the valve cycle for the SI and CI engines, the steady solutions are mapped by two points. The last graph compares the pressure along the streamline (see Fig. 4) for the unsteady (Fig. 8e) and steady (Fig. 9b) computations at the same valve lift 7 mm.

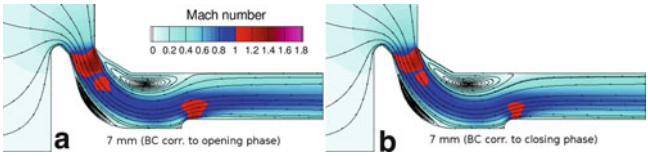

Fig. 9 Steady results. Boundary conditions correspond to CI engine at valve lift 7 mm in the opening (left) and the closing phase. Contours of Mach number, velocity streamlines

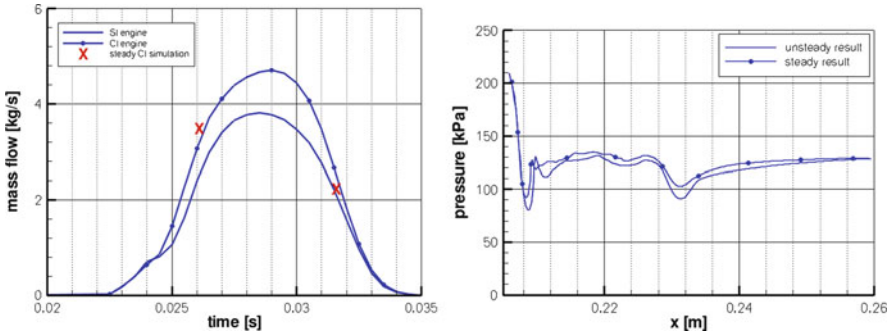

Fig. 10 Comparison of the SI and CI engine model: mass flow rate (left). Comparison of the unsteady and steady model: pressure development in the exhaust pipe (right)

6 Conclusions

The steady results have shown similar behaviour for all the turbulence models tested.

The flowfield of unsteady results are in qualitative agreement with equivalent steady solutions, however, the mass flow rate can differ up to approximately 10% (see Fig. 10). Also the pressure development along the mean streamline behind the channel throat differs from the steady state.

In case of the CI engine (due to higher inlet pressure) one observes the aerodynamical choking and larger supersonic regions, compared to the SI engine. The SI model is choking-free in the dominant time of the valve cycle. The negligible mass flow in the early and late stages of the valve cycle also justifies the use of grids with minimal (non-zero) valve opening. The oncoming work will be aimed at more advanced turbulence models for the unsteady simulations, flow characteristics at different rpm and mainly on 3D unsteady simulations.

Acknowledgements This work has been supported by the grant of the Czech Science Foundation No. P101/10/1329 and by the project 1M6840770002 Josef Božek Research Center of the Ministry of Education of the Czech Republic.

References

1. COOLFluiD homepage [on-line], http://coolfluidsrv.vki.ac.be, Cited 17 Feb 2011
2. Barth, T. J., Jesperson, D. C.: The design and application of upwind schemes on unstructured meshes. AIAA Paper **89(0366)** (1989)
3. Favre, A.: Equations des gaz turbulents compressibles. J. de Mecanique **4**, 361–421 (1965)
4. Heywood, J. B.: Internal Combustion Engine Fundamentals. McGraw-Hill, Inc. USA (1988)
5. Lani, A.: An Object Oriented and High Performance Platform for Aerothermodynamics Simulation. Doctoral thesis, VKI, Belgium (2009)
6. Liou M. S.: A sequel to AUSM, Part II: AUSM$^+$up for all speeds, J. of Computational Physics **214**, 137–170 (2006)
7. Menter, F. R., Rumsey, C. L.: Assessment of Two-Equation Turbulence Models for Transonic Flows. AIAA 25th Fluid Dynamics Conference, Colorado Springs, USA (1994)
8. Menter, F. R.: Two-Equation Eddy-Viscosity Turbulence Models for Engineering Applications, AIAA Journal **32-8** (1994)
9. Michler, C.: Development of an ALE Formulation for Unsteady Flow Computations on Moving Meshes using RD Schemes, Project Report **2000-13**, VKI, Belgium (2000)
10. S. Wallin: Engineering turbulence modelling for CFD with focus on explicit algebraic Reynolds stress models. Dissertation Thesis, Norsteds Tryckeri AB, Sweden (2000)
11. D. C. Wilcox, Formulation of the $k - \omega$ Turbulence Model Revisited, AIAA J. **46-11** (2008)

The paper is in final form and no similar paper has been or is being submitted elsewhere.